Atomistic simulations of aromatic polyurea and polyamide for capacitive energy storage

Rui Dong, V. Ranjan, Marco Buongiorno Nardelli, and J. Bernholc

Phys. Rev. B **92**, 024203 — Published 31 July 2015

DOI: 10.1103/PhysRevB.92.024203

Atomistic Simulations of Aromatic Polyurea and Polyamide for Capacitive Energy Storage

Rui Dong,[1] V. Ranjan,[1] Marco Buongiorno Nardelli,[1,2] and J. Bernholc[1]

[1]*Department of Physics, North Carolina State University, Raleigh, NC, 27695, USA*

[2]*Department of Physics and Department of Chemistry, University of North Texas, Denton, TX 76203, USA*

Materials for capacitive energy storage with high energy density and low loss are desired in many fields. We investigate several polymers with urea and amide functional groups using density functional theory and classical molecular dynamics simulations. For aromatic polyurea (APU) and para-aramid (PA), we find several nearly energetically-degenerate ordered structures, while meta-aromatic polyurea (mAPU) tends to be rotationally disordered along the polymer chains. Simulated annealing of APU and PA structures result in the formation of hydrogen-bonded sheets, highlighting the importance of dipole-dipole interactions. In contrast, hydrogen bonding does not play a significant role in mAPU, hence the propensity to disorder. We find that the disordered structures with misaligned chains have significantly larger dielectric constants, due to significant increase in the free volume, which leads to easier reorientation of dipolar groups in the presence of an electric field. Large segment motion is still not allowed below the glass transition temperature, which explains the experimentally observed very low loss at high field and elevated temperature. However, the degree of disorder needs to be controlled, because highly entangled structures diminish the free dipoles and decrease permittivity. Among the considered materials, mAPU is the most promising dielectric for capacitive energy storage, but the concept of increasing permittivity while maintaining low loss through disorder-induced free volume increase is generally applicable and provides a new pathway for the design of high-performance dielectrics for capacitive energy storage.

I. Introduction

In the quest for quickly storing and releasing electrical energy, capacitors stand apart both by releasing energy 300-2000 times faster [1] than batteries and by being able to undergo ~10^6 charge-discharge cycles, in contrast to ~10^3 for batteries. However, the maximum density of energy stored in capacitors is much lower than that of batteries, hence the quest for better dielectric materials with much higher effective dielectric constant. Among candidate dielectrics, polymers are particularly attractive because of their high breakdown strength, *gentle failure*, *i.e.*, remaining insulators even at breakdown, easy processability and light weight. However, the state-of-the-art commercial polymer for energy storage, biaxially oriented polypropylene (BOPP) has a dielectric constant of only 2.2 [2]. With the low permittivity, the energy density is only moderate at 4 J/cm^3. Although the loss in BOPP is very low (0.02%) at moderate electric fields [3], the conduction loss increases significantly at high field [4], and operating temperatures above 85℃ reduce the breakdown strength [5].

Both experimental and computational efforts have been devoted to finding new polymers with enhanced properties. One route is the ferroelectric copolymer/terpolymer system based on polyvinylidene fluoride (PVDF) [6–9], which have a dielectric constants of 10-50. In particular, polymers of VDF and "defect" co-polymers chlorotrifluoroethylene (CTFE) or hexafluoropropylene (HFP) have energy densities greater than 18 J/cm^3 [6,8], far more than PVDF alone. Our previous work uncovered the reason for this enhancement: a reversible, non-polar to polar phase transition occurs as high electric field is applied and then released [7]. In PVDF with low copolymer concentration (<20%), the non-polar α phase has the lowest energy, but the polar β phase

is preferred in high electric field. The electric displacement *D* increases non-linearly during the non-polar to polar phase transition, which leads to the ultra-high energy density. A geometrical transition pathway with low energy barrier that makes the transition thermally accessible was identified [9]. The role of the copolymers is both to lower the activation energies and to nano-structure the polymer into domains, enabling a gradual and smooth transformation. Other copolymers, such as tetrafluoroethylene (TeFE) [10], trifluoroethylene(TrFE) [11] and their combinations have been tested experimentally to maximize the dielectric performance. However, the PVDF-based systems are not suitable for working temperatures higher than 150 ℃, and they exhibit unacceptably high losses due to remanent polarization. Recently, an alternative route to high performance dielectric polymers was discovered [12–14]: the aromatic polyurea/polythiourea family of polymers have permittivities of 4.2-5.6 in broad temperature and frequency ranges, and they have significantly lower losses at high field than BOPP. Polyureas have already been widely used in industry, in applications focusing on their great elasticity and strength. Moreover, aromatic polyureas have been reported to have sizable pyroelectric, piezoelectric and nonlinear optical properties more than a decade ago [15–19], suggesting their potential as capacitive dielectrics. All polymers in this family have functional groups with large dipole moments, *i.e.*, urea, thiourea and amide, but they do not form a ferroelectric phase as PVDF-based materials do. This aspect eliminates a large potential factor for loss. The polyureas act thus as linear dielectric materials, in which the relation between the energy density *U* and the applied electric field *E* is simply $U = \frac{1}{2}\varepsilon_0\varepsilon_r E^2$, where ε_0 is the vacuum permittivity, and ε_r is the relative permittivity. Therefore, the relative permittivity ε_r is the key to high energy density.

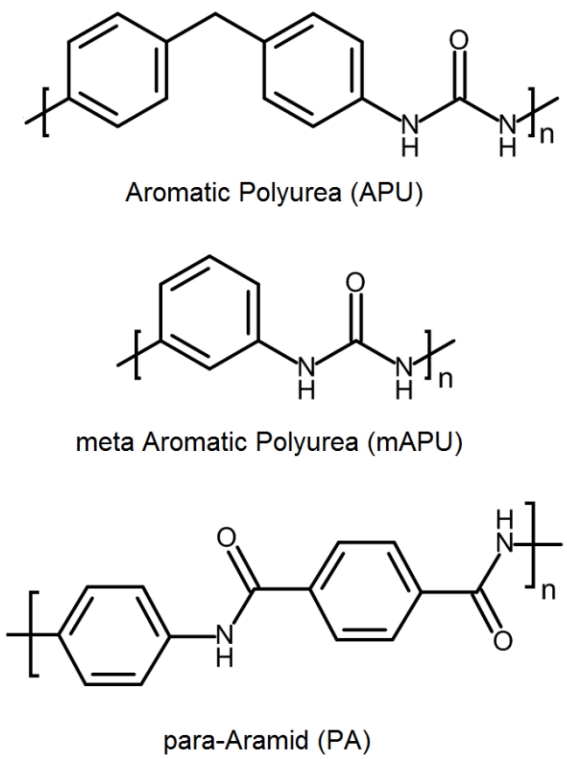

FIG. 1. Schemes of polymers investigated here: aromatic polyurea, meta-aromatic polyurea, and para-aramid.

In this work, we study three members in the aromatic polyurea family, aromatic polyurea (APU) [13], meta-aromatic polyurea (mAPU) [14] and para-aramid (PA). Their chemical formulas are shown in Fig. 1. We use atomistic simulations, combining results from both density functional theory (DFT) and classical molecular dynamics (MD) to search for the relation between microscopic structures and the dielectric properties. Significantly, we find larger dielectric constants in structures that either are disordered with partially misaligned chains or blended into nano domains. However, substantial entanglement has a negative effect on permittivity, due to a reduced number of large effective dipole groups. This indicates that the degree of disorder needs to be controlled. We attribute the enhancement of the dielectric response to disorder-induced increase in the specific volume, compared to ordered crystal-like structures. The larger free volume

leads to easier re-orientation of the dipolar functional groups in response to an external field, and therefore to a larger permittivity. Our findings demonstrate a promising way to enhance the permittivities of linear dielectrics without introducing high loss.

The rest of the paper is organized as follows: Section II describes the theoretical background and computational details, Section III presents the results and discussion, while Section IV contains summary and conclusions.

II. Theory and computational details

A. Theoretical background

In this work we focus on calculation of ε_r, so we omit the subscript "r" in the following. In general, permittivity is a complex and frequency-dependent quantity

$$\varepsilon(\omega) = \varepsilon_1(\omega) - i\varepsilon_2(\omega), \tag{1}$$

where ε_1 and ε_2 are real and ε_2 is the dielectric loss. In anisotropic materials, permittivity is a complex tensor that depends on the orientations of the field and the sample. The elements of the static permittivity tensor $\varepsilon_{\alpha\beta}(0)$ have both electronic and ionic contributions, which can be expressed as [20–24]

$$\varepsilon_{\alpha\beta}(0) - \varepsilon_{\alpha\beta}(\infty) = \frac{4\pi}{\Omega k_B T}\mathcal{M}_{\boldsymbol{\alpha\beta}}, \tag{2}$$

where α and β stand for the three Cartesian directions, $\varepsilon_{\alpha\beta}(\infty)$ is the electronic dielectric constant, Ω is the volume of simulation supercell, k_B is Boltzman constant, and T is temperature. $\mathcal{M}_{\boldsymbol{\alpha\beta}}$ is the covariance of two dipole moment components,

$$\mathcal{M}_{\alpha\beta} = \langle M_\alpha M_\beta \rangle - \langle M_\alpha \rangle \langle M_\beta \rangle. \tag{3}$$

In molecular dynamics (MD) simulation with charged atoms, $M_{\boldsymbol{\alpha}} = \sum_i q_i r_{i\boldsymbol{\alpha}}$ is the dipole moment in α-direction, q_i is the charge and $r_{i\boldsymbol{\alpha}}$ is the α coordinate of atom i. The summation is over all atoms in the simulation cell. The dipole moment M can be obtained from MD simulation in the canonical ensemble. The frequency dependent permittivity $\varepsilon_{\alpha\beta}(\omega)$ can then be extracted by Fourier-transforming the cross-covariance of time-dependent dipole moments

$$\epsilon_{\alpha\beta}(\omega) = \epsilon^0_{\alpha\beta} - \frac{4\pi}{\Omega k_B T} i\omega \int_0^\infty e^{-i\omega t} \mathcal{M}_{\alpha\beta}(t) dt, \tag{4}$$

where $\mathcal{M}_{\alpha\beta}(t) = \langle M_\alpha(0) M_\beta(t) \rangle - \langle M_\alpha \rangle \langle M_\beta \rangle$. The imaginary part of $\varepsilon_{\alpha\beta}(\omega)$ is the loss.

B. Computational details.

The classical MD code LAMMPS [25] is used in this work, with force field reaxFF. We employ different force fields for urea-based polymers [26] and amide-based polymers [27]. The use of reaxFF is essential in our simulations, because it is able to capture the variation of atomic charges and thus results in a more realistic dielectric response, and charge variation affects the total dipole moment. Simulated annealing is used to obtain microscopic structures with the following schedule: 600 K equilibration of 1 ns in the *NPT* ensemble, cooling to 300 K at the rate of 25 K/100 ps, and equilibration time of 1 ns at 300 K in the *NPT* ensemble. Nosé-Hoover thermostat [28,29] is used for temperature and pressure control with the target pressure set to 0. The time step is fixed at 0.5 fs throughout the MD simulation. Our simulation cell contains 8 independent polymer chains and each chain has 8 monomers. The chains extend periodically through the system. For different polymers, this simulation cell has 896 to 1024 atoms in total. In the final run of 1 ns at 300K, the dipole moment $\vec{M}$ is sampled every 10 fs in the *NVT* ensemble.

In the DFT part of our simulation, the plane wave code Quantum Espresso [30] is employed. We choose ultrasoft [31] pseudopotentials with exchange-correlation functional PBE+D [32,33]. Energy cutoffs of 35 and 420 Rydbergs are used for electron wave functions and electron charge density, respectively. To save the computational time in the DFT part, a smaller simulation cell with 2 infinite chains with 4 monomers each is used. After optimization, all force components are smaller than 0.01 eV/$Å^3$, and the cell parameters are relaxed until all stress components are smaller than 0.5 KBar. The electronic permittivity tensor for the lowest energy structure is obtained from density functional perturbation theory (DFPT) [34].

C. Effects of cell size and interatomic potential

Based on the methodology described above, the ionic permittivity is calculated in two mAPU simulation cells, containing 8 and 64 monomers, respectively. Fig. 2 (a) shows the convergence of Eq. (2) vs. simulation time in the two cells. Fig. 2(b) shows the thermal loss in the two cells at very low frequencies. The thermal loss at very low frequencies should be close to 0, because atomic motions have much higher frequencies. While the use of the 8-monomer cell results in high noise level, the noise in low frequency loss in the 64-monomer cell is very small. Part of the reason is that the geometry is artificially constrained in the small cell. Fig. 3 compares the atomic configurations in the two cells. The 64-monomer cell has a more realistic geometry. The neighboring urea units are close to each other because the strong dipole-dipole interaction lowers the total energy. On the other hand, the phenylene groups do not favor being in close proximity to each other. Therefore, each phenylene group is in the middle of two phenylene groups of the next chain. However, such configuration is not accessible in the small 8-monomer cell. Because there are only two independent chains, chains 1 and 3 have to be identical. Due to the more favorable packing, the 64-monomer unit cell has total energy 5.6 meV/atom lower than the 8-monomer cell.

Moreover, the average ionic permittivity of 64-monomer unit cell is 0.8 higher than that of the small cell. To show the difference is due to different geometries instead of a size effect, we calculated the ionic permittivity of a 32-monomer unit cell. It captures the same geometry as the 64-monomer unit cell. The spherically averaged permittivity is 2.69, which differs by less than 0.2 from the 64-monomer result. These results show that a realistic geometry is very important for calculating ionic dielectric properties.

Turning to electronic permittivities, the 8-monomer cell has $\varepsilon_{xx}(\infty)$=3.09, $\varepsilon_{yy}(\infty)$=2.63, $\varepsilon_{zz}(\infty)$=4.36, and $\varepsilon_{avg}(\infty)$=3.36. The 64-monomer cell has $\varepsilon_{xx}(\infty)$=2.66, $\varepsilon_{yy}(\infty)$=3.11, $\varepsilon_{zz}(\infty)$=4.45, and $\varepsilon_{avg}(\infty)$=3.41. The difference between spherically averaged permittivities is smaller than 0.1. It indicates that the electronic permittivity is not sensitive to the packing of polymer chains. Therefore, we use the small unit cell to calculate electronic permittivities for the systems considered here.

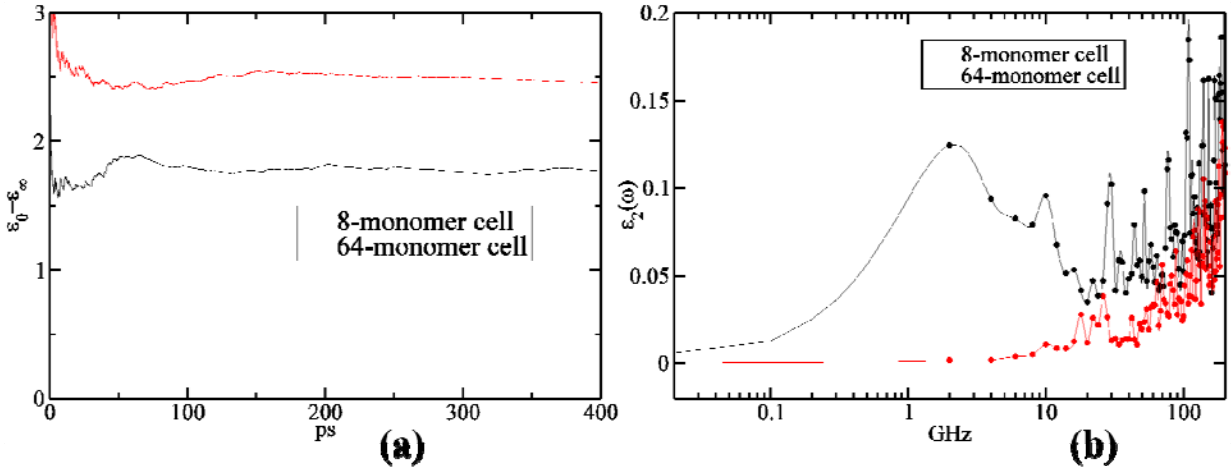

FIG. 2. (a) The convergence of ionic permittivity, Eq. (2), vs. simulation time of 8-monomer and 64-monomer mAPU cells. (b) The low frequency thermal loss in 8-monomer and 64-

monomer mAPU cells. A damping function $\mathrm{f(t)} = \exp(-0.005\mathrm{t})$ is applied to the cross-covariance $\mathcal{M}_{\alpha\beta}(t)$ in Eq. (4) to avoid finite time artifacts, such as negative loss.

According to Eq. (2), dipole moment variation is the source of ionic permittivity. Therefore, capturing the variation of atomic charge is essential in simulations. To demonstrate the effect of varying charge, we performed tests in the ordered structures of APU and mAPU. The averaged charges $\langle q_i \rangle$ of each atom are calculated in the *NVT* ensemble during the sampling period. We then use the average values $\langle q_i \rangle$ instead of $q_i(t)$ to calculate the dipole moment. The results are shown in Table I. The ionic permittivity calculated using the fixed charges is one order of magnitude smaller than the one calculated with the varying charges. This is the reason we choose reaxFF, although it is much more expensive than a fixed-charge force field.

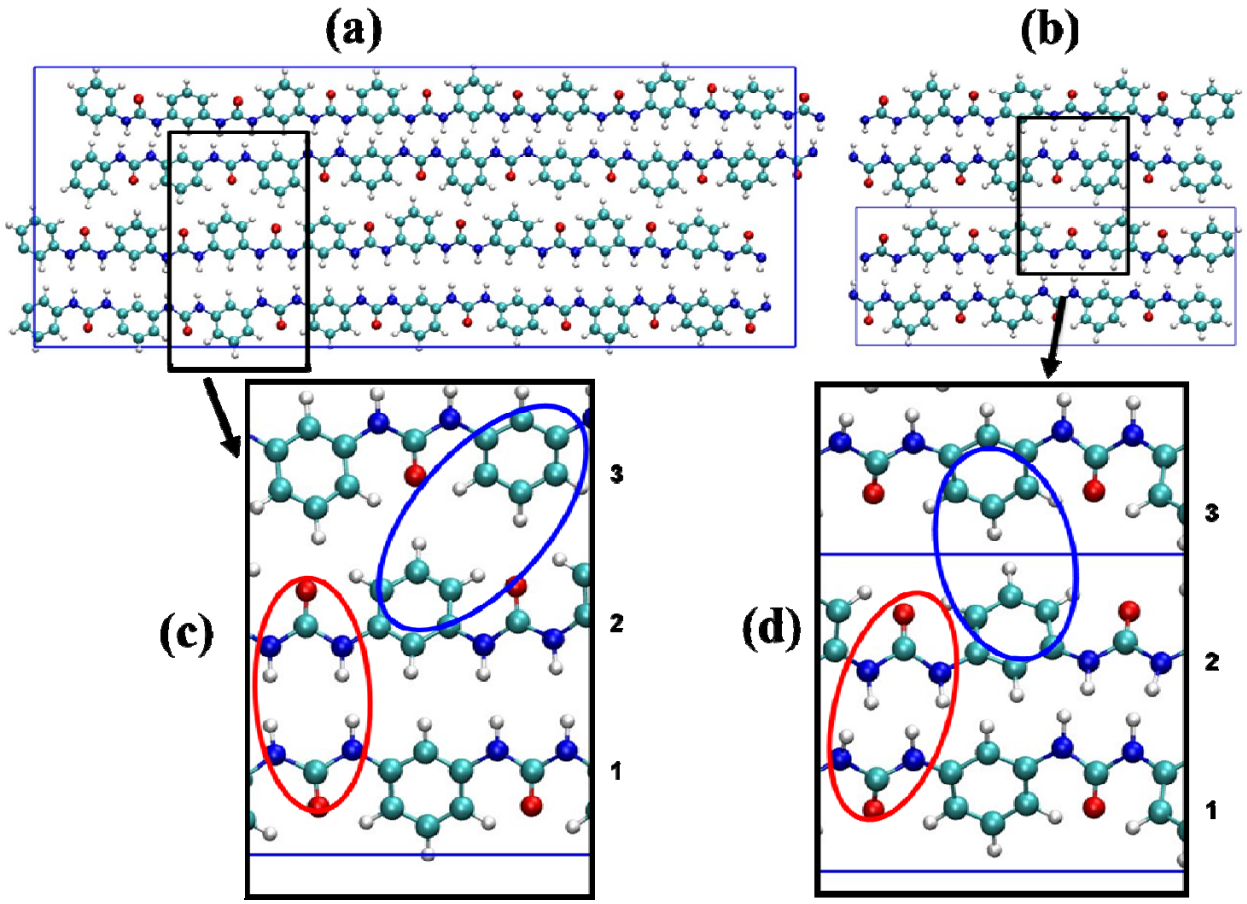

FIG. 3. Local arrangement of dipole pairs and phenylene groups in 8-monomer and 64-monomer unit cells. The blue line indicates unit cell boundaries. (a) The top view of the 64-monomer unit cell. (b) The top view of the 8-monomer unit cell. (c) Zoomed-in partial view of the 64-monomer unit cell. The urea units form antiparallel pairs, while the phenylene groups mi-salign along the chains. (d) Zoomed-in partial view of the 8-monomer unit cell. The urea units form antiparallel pairs, but the phenylene groups are aligned because chains 1 and 3 are identical.

TABLE I. Ionic permittivity of APU and mAPU calculated with varying and fixed charges. See text.

	$\varepsilon_{avg}(ionic)$ in ordered structure

	mAPU	APU
Varying charge	2.51	1.96
Fixed charge	0.35	0.27

III. Results and Discussion

To search for possible ordered structures, four initial guesses of geometries are created, as displayed in Fig. 4. Since all the polymers have dipolar functional groups, the dipole moments in chains can be arranged parallel or antiparallel. The chains can also be shifted along the z-axis to align two neighboring urea units or to alternate them. The four starting geometries are arranged with: a) parallel chains and aligned polar units; b) antiparallel chains and aligned polar units; c) parallel chains and alternating polar units; and d) antiparallel chains and alternating polar units.

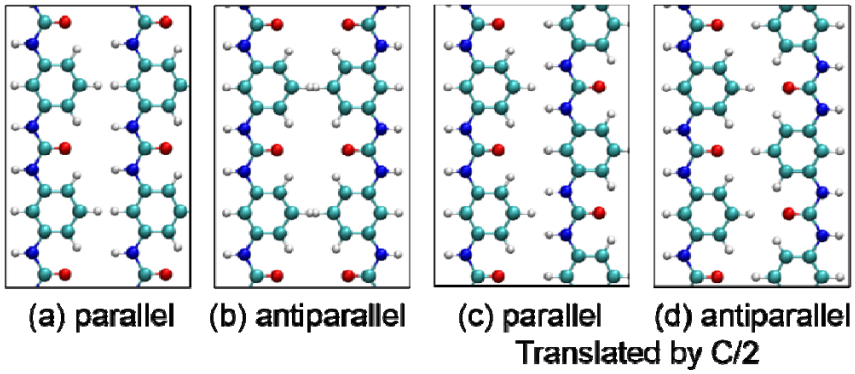

FIG. 4. Starting geometries of ordered mAPU simulation cells. Color code: white - hydrogen, green - carbon, blue - nitrogen, red - oxygen. (a) Parallel-aligned dipoles. (b) Antiparallel-aligned dipoles. (c) Parallel-shifted dipoles. (d) Antiparallel-shifted dipoles.

After simulated annealing, several ordered crystal-like structures are found for these polymers. We obtain four different ordered structures for APU, shown in Fig. 5(a)-(d). The energy differ-

ence between the four structures is ~20 meV/atom in reaxFF and only ~4 meV/atom at the DFT level. The lowest energy structure has urea units with the anti-parallel arrangement. Interestingly, only one of the four starting mAPU geometries converges to an ordered crystal-like structure, which is shown in Fig. 5(e). The other three converge to disordered structures, in which the chains are misaligned in the xy-plane, as shown in Fig. 5(f)-(h). The disordered structures still have infinite polymer chains along the z-axis. There is no entanglement between the chains and the structures are still highly anisotropic. The three misaligned structures have total energies ~20 meV/atom higher than the ordered structure in reaxFF, similar to the energy variation between ordered APU structures. The four starting geometries of PA converge to two different ordered structures. The energy difference is ~6 meV/atom in reaxFF and <1 meV/atom at the DFT level. Uniquely among the polymers studied in this work, PA has dipolar amide linkers pointing in opposite directions in the same chain. Therefore, regardless of inter-chain arrangements, PA has an antiparallel structure and zero spontaneous polarization. We thus find that the lowest energy structures of APU, mAPU and PA all have zero spontaneous polarization, in agreement with experiments [13,14].

Many of the APU and PA ordered structures arrange into sheets. The dipolar functional groups form hydrogen bonds linking neighboring chains, and the linked chains form hydrogen-bonded sheets (H-sheets). H-sheets of APU and PA are shown in Fig. 6. However, the only mAPU ordered structure does not have such nanostructure. Instead, the ureas form antiparallel dipole pairs as shown in Fig. 3. Therefore, the interactions between nearby dipoles in mAPU are weaker than those in APU and PA. The tendency of mAPU to be disordered is facilitated by weaker interactions between the dipole units.

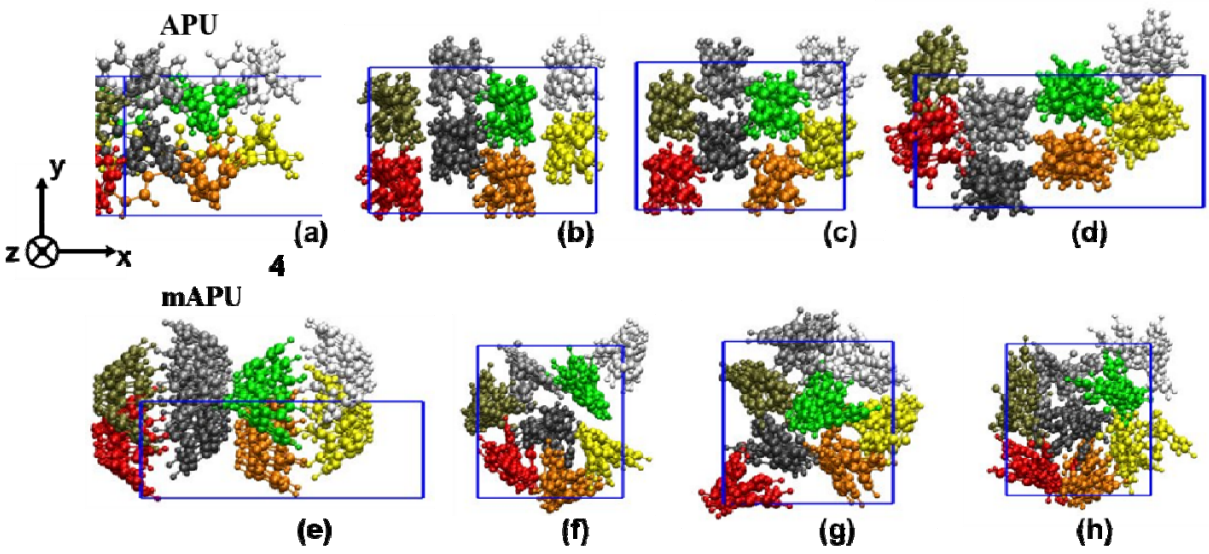

FIG. 5. Front view of APU, (a)-(d), and mAPU, (e)-(h), supercells. The polymer chains are along the *z* axis. Colors represent different polymer chains. (a)-(e): ordered crystal-like structures, where polymer chains occupy sites on a "lattice." (f)-(h): disordered structures with misaligned chains.

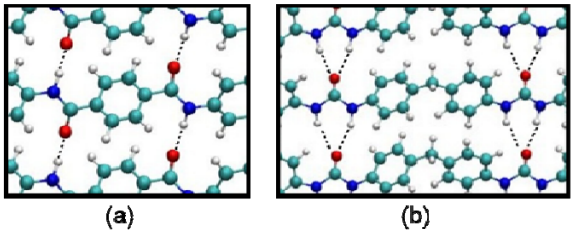

FIG. 6. The hydrogen-bonded sheets in ordered structures of: (a) PA and (b) APU. Dashed lines indicate hydrogen bonds between dipolar groups.

The ionic and electronic contributions to the dielectric constants of the ordered structures, calculated according to the methodology described in Sec. II, are listed in Table II. For the polymers that have more than one ordered structure, the lowest energy one is selected. As mentioned in Sec. II, the spherically averaged electronic permittivities are similar for all the studied struc-

tures of each polymer. It shows that the electronic permittivity does not depend on the packing and arrangement of individual chains. However, the ionic contributions strongly depend on atomic geometries.

TABLE II. Calculated electronic, ionic and total permittivities of APU, mAPU and PA.

	APU	mAPU	PA
$\epsilon_{xx}(\infty)$; $\epsilon_{yy}(\infty)$; $\epsilon_{zz}(\infty)$	2.93; 3.05; 4.10	3.09; 2.63; 4.36	2.49; 3.42; 5.49
$\epsilon_{avg}(\infty)$	3.36	3.36	3.8
$\epsilon_{avg}(ionic)$	1.96	2.51	1.12
$\epsilon_{avg}(0)$	5.32	5.87	4.92
Exp.	~4.2 (Ref. [13])	~5.6 (Ref. [14])	

Moreover, we find that the misaligned disordered structures of mAPU have significantly larger ionic permittivities than the ordered one. The average ionic contribution and total dielectric constant of disordered mAPU structures are listed in Table III. The reasons for enhancement are explained in Ref. [35]: The three misaligned structures have specific volumes ~12% larger than the ordered structure. In particular, dipole reorientation is facilitated by the larger free volume, enhancing permittivity. Suppression of periodicity also allows for lower frequency optical phonons, which enlarge the dielectric constant. However, the polymer chains are still closely packed and large segment motion, which would lead to high loss, is not feasible.

To confirm that the enhancement is induced by disorder, we study similar effects in APU and PA. For these two polymers, a disordered structure cannot be obtained from annealing. Therefore, we artificially create a mixture of the four starting geometries shown in Fig. 4. To test the reliability of this procedure, we also use it to create a mixed structure of mAPU. The same simulated annealing procedure is applied to the mixtures before calculating the ionic permittivities.

The ionic and total permittivities of the blended structures are shown in Table III. The test for the blended mAPU structure suggests that this approach is reasonable, because it leads to the same total energy and similar ionic permittivity as for the annealed single structures. A similar enhancement of ionic permittivities for the blended structures is also found in APU and PA, *cf.* Tables II and III. These results unequivocally show that the enhancement in ionic permittivity is due to disorder, either thermally induced or through the formation of nano domains. This enhancement suggests a new way to increase the dielectric constant while avoiding high loss due to large segment motion.

Table III. Properties of disordered structures of APU, mAPU and PA. The electronic contribution is taken to be the same as in Table II. ΔE_{total} is calculated with reference to the lowest energy ordered structure.

	mAPU(annealed)	mAPU(mixed)	APU(mixed	PA(mixed)
$\boldsymbol{\epsilon}_{avg}(ionic)$	3.86	4.17	2.9	4.1
$\boldsymbol{\epsilon}_{avg}(0)$	7.22	7.53	6.26	7.9
ΔE_{total}[meV]	+20	+20	+8	+12

The larger ionic permittivity in disordered structures motivated us to study a highly entangled model, which has an even larger degree of disorder. A simulation cell is prepared where a random coil consisting of a finite 100-monomer mAPU chain and its replicas fill the entire space. The same simulated annealing procedure is applied. After annealing, the highly entangled disordered structure has a similar specific volume as the misaligned disordered structures, but it is essentially isotropic. The annealed unit cell with a fully unwrapped chain is shown in Fig. 7. However, the ionic permittivity of the highly entangled structure is just 2.2, compared to the 3.86 average of the misaligned structures.

In the misaligned structures, all polymer chains are still essentially straight and uniaxial. The urea units are all in the same configuration shown in Fig. 8(a), which has the maximum dipole moment because the dipoles of the C=O bond and the two N-H bonds point in the same direction. However, the polymer chain in the highly entangled structure has many turning points. At the turning points, reorientation of bonds reduces the dipole moments of the urea units. Figs. 8(b)-(d) show three urea configurations with reduced dipole moment. The dielectric responses of these dipole units are thus less effective. We conclude that a larger free volume and a disordered geometry are needed to enhance the ionic permittivity. At the same time, entanglement of the chains should be avoided to maintain the maximum number of effective dipolar units.

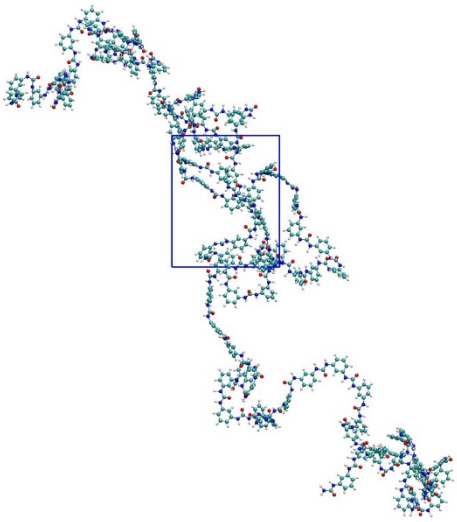

FIG. 7. Highly entangled structure of mAPU after simulated annealing. The blue box indicates the unit cell boundaries.

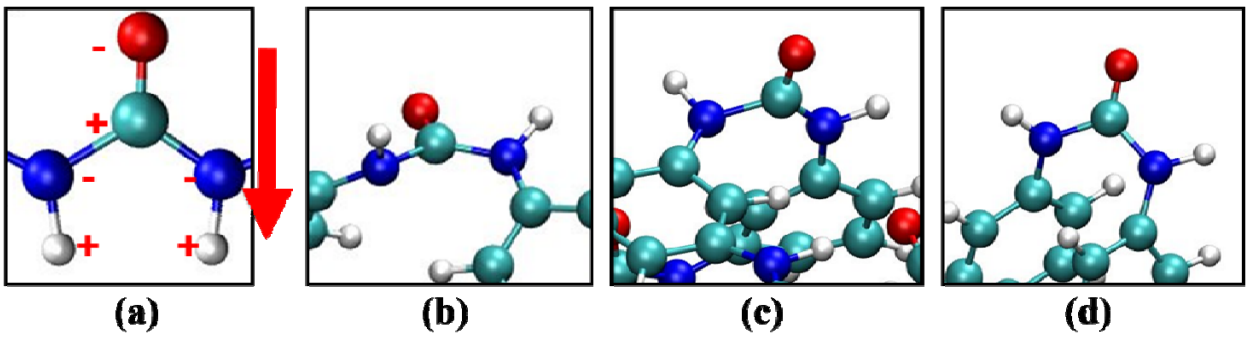

FIG. 8. (a) The configuration of urea groups in ordered and misaligned structures of mAPU. It has the maximum dipole moment in both cases. (b)-(c) Configurations of urea groups at the turning points of the highly entangled disordered structure. They all have reduced dipole moments.

Comparing the results for the ordered (Table II), misaligned (Table III) and entangled structures to experimental values also listed in Table II, we note that the theoretical values do not fully reproduce the experimental ones. There are several potential sources of errors. The electronic permittivities, calculated from first-principles by DFT, are probably quite accurate. The ionic permittivities, calculated using the variable-charge reaxFF force field, are likely to be less precise. The variable charge aspect, as shown in Table I, is important, because the ionic permittivities calculated with the fixed-charge potential are unphysically small. However, the largest source of discrepancy between the theoretical and experimental results is likely due to differences in structures. The theoretical unit cells contain up to ~1000 atoms and are annealed for ~ 1ns. The experimental polymer chains contain thousands of atoms each and the film deposition times are obviously far longer. Furthermore, the experimental structures may consist of different nano and micro domains: ordered, misaligned and entangled. Nevertheless, the simulations clearly reproduce the experimental trends in permittivity and the well-known tendency of para-aramid to

form hydrogen-bonded sheets. The disorder-induced increase in permittivity, discovered through simulations, has also been confirmed experimentally [35].

IV. Summary and Conclusions

We have investigated the dielectric properties of different microscopic geometries of three urea/amide based aromatic polymers using atomistic simulations: aromatic polyurea (APU), meta-aromatic polyurea (mAPU), and para-aramid (PA). In all three cases, the average electronic permittivity is largely independent of the detailed atomic arrangement of the chains. However, ionic permittivity is closely related to the microscopic geometry. A realistic geometry is thus very important for calculating the dielectric properties.

The ionic part of the dielectric constant has been calculated using molecular dynamics with the interatomic force-field potential reaxFF. In order to obtain reliable results for these highly dipolar polymers, it is essential to use variable-charge potentials.

Several starting geometries have been used to form polymer models to be optimized by simulated annealing. For APU and PA, simulated annealing resulted in various energetically-close ordered structures. Their calculated dielectric constants agree well with experimental data. For mAPU, we uncovered a strong propensity for disordered structures with misaligned chains, due to weaker dipole-dipole interaction. The misaligned structures have significantly higher ionic permittivities than an ordered mAPU structure. The main reason for the enhancement is the larger free volume introduced by the disorder, which enables greater reorientation of dipolar groups as the electric field is applied. Moreover, disorder allows for lower frequency phonons, which also increases the ionic permittivity. Our studies of blended APU and PA structures consisting of different nano-domains further confirm that the enhancement is due to disorder. One should

stress that the above mechanism of enhancing the ionic permittivity by increasing the free volume does not lead to large segment motion. Therefore, it does not introduce high loss. However, we also find that in highly entangled mAPU structures, which have much greater disorder, the ionic permittivity is somewhat smaller than that of the ordered structure, although their specific volumes are similar to the misaligned structures. The lack of enhancement can be explained by the fact that entanglement leads to many turning points along the chains, and the urea units at the turning points have configurations with reduced dipole moments. These are less effective in responding to the electric field, hence a smaller dielectric constant. Our results thus suggests that entanglement of polymer chains should be reduced to a minimum, while still introducing rotational disorder along the chains.

Our findings suggest a different path to optimization of polymer dielectrics that could lead to much enhanced dielectric materials. Among the three polymers that we have studied, mAPU is the best candidate for energy storage due to its large dipole density and easy formation of the disordered structure.

V Acknowledgements

We thank Prof. Qiming Zhang from Penn State Univ. for sharing data with us and for many discussions. This work is supported by ONR grants N00014-14-1-0106 and N00014-13-1-0719. Supercomputer simulations were performed at DoD Supercomputing Centers and at Blue Waters supercomputer at NCSA, supported by NSF grant OCI-1036215.

References

[1] P. Flynn, *Meeting the Energy Needs of Future Warriors* (National Academies Press, Washington D.C., 2004).

[2] M. Rabuffi and G. Picci, Status quo and future prospects for metallized polypropylene energy storage capacitors, IEEE Trans. Plasma Sci. **30**, 1939 (2002).

[3] H. W. Starkweather, P. Avakian, R. R. Matheson, J. J. Fontanella, and M. C. Wintersgill, Ultralow temperature dielectric relaxations in polyolefins, Macromolecules **25**, 6871 (1992).

[4] K. C. Kao, *Dielectric Phenomena in Solids* (Elsevier Academic Press, London, UK, 2004).

[5] J. Ho and R. Jow, *Characterization of High Temperature Polymer Thin Films for Power Conditioning Capacitors* (Army Research Laboratory, Adelphi, US, 2009).

[6] B. Chu, X. Zhou, K. Ren, B. Neese, M. Lin, Q. Wang, F. Bauer, and Q. M. Zhang, A Dielectric Polymer with High Electric Energy Density and Fast Discharge Speed, Science **313**, 334 (2006).

[7] V. Ranjan, L. Yu, M. Buongiorno Nardelli, and J. Bernholc, Phase Equilibria in High Energy Density PVDF-Based Polymers, Phys. Rev. Lett. **99**, 047801 (2007).

[8] X. Zhou, X. Zhao, Z. Suo, C. Zou, J. Runt, S. Liu, S. Zhang, and Q. M. Zhang, Electrical breakdown and ultrahigh electrical energy density in poly(vinylidene fluoride-hexafluoropropylene) copolymer, Appl. Phys. Lett. **94**, 162901 (2009).

[9] V. Ranjan, M. Buongiorno Nardelli, and J. Bernholc, Electric Field Induced Phase Transitions in Polymers: A Novel Mechanism for High Speed Energy Storage, Phys. Rev. Lett. **108**, 087802 (2012).

[10] S. Zhang, C. Zou, D. I. Kushner, X. Zhou, R. J. Orchard, N. Zhang, and Q. M. Zhang, Semicrystalline polymers with high dielectric constant, melting temperature, and charge-discharge efficiency, IEEE Trans. Dielectr. Electr. Insul. **19**, 1158 (2012).

[11] L. Zhu and Q. Wang, Novel Ferroelectric Polymers for High Energy Density and Low Loss Dielectrics, Macromolecules **45**, 2937 (2012).

[12] S. Wu, W. Li, M. Lin, Q. Burlingame, Q. Chen, A. Payzant, K. Xiao, and Q. M. Zhang, Aromatic Polythiourea Dielectrics with Ultrahigh Breakdown Field Strength, Low Dielectric Loss, and High Electric Energy Density, Adv. Mater. **25**, 1734 (2013).

[13] Y. Wang, X. Zhou, M. Lin, and Q. M. Zhang, High-energy density in aromatic polyurea thin films, Appl. Phys. Lett. **94**, 202905 (2009).

[14] S. Wu, M. Lin, Q. Burlingame, and Q. Zhang, Meta-aromatic polyurea with high dipole moment and dipole density for energy storage capacitors, Appl. Phys. Lett. **104**, 072903 (2014).

[15] Y. Takahashi, M. Iijima, and E. Fukada, Pyroelectricity in Poled Thin Films of Aromatic Polyurea Prepared by Vapor Deposition Polymerization, Jpn. J. Appl. Phys. **28**, L2245 (1989).

[16] Y. Takahashi, S. Ukishima, M. Iijima, and E. Fukada, Piezoelectric properties of thin films of aromatic polyurea prepared by vapor deposition polymerization, J. Appl. Phys. **70**, 6983 (1991).

[17] H. S. Nalwa, T. Watanabe, A. Kakuta, A. Mukoh, and S. Miyata, Aromatic polyureas: a new class of nonlinear optical polymer with large second-harmonic generation, Electron. Lett. **28**, 1409 (1992).

[18] M. Iijima, G. H. Shen, Y. Takahashi, E. Fukada, A. Tanaka, and S. Sakata, Characteristics of pyroelectric sensors of polyurea films prepared by vapor deposition polymerization, Thin Solid Films **272**, 157 (1996).

[19] X.-S. Wang, Y. Takahashi, M. Iijima, and E. Fukada, Dielectric Relaxation in Polyurea Thin Films Prepared by Vapor Deposition Polymerization, Jpn. J. Appl. Phys. **33**, 5842 (1994).

[20] R. Kubo, Statistical-Mechanical Theory of Irreversible Processes. I. General Theory and Simple Applications to Magnetic and Conduction Problems, J. Phys. Soc. Jpn. **12**, 570 (1957).

[21] H. Frohlich, *Theory of Dielectrics: Dielectric Constant and Dielectric Loss*, 2 edition (Oxford University Press, Oxford, 1987).

[22] M. Neumann, Dipole moment fluctuation formulas in computer simulations of polar systems, Mol. Phys. **50**, 841 (1983).

[23] M. Neumann and O. Steinhauser, On the calculation of the dielectric constant using the Ewald-Kornfeld tensor, Chem. Phys. Lett. **95**, 417 (1983).

[24] M. Neumann and O. Steinhauser, On the calculation of the frequency-dependent dielectric constant in computer simulations, Chem. Phys. Lett. **102**, 508 (1983).

[25] S. Plimpton, Fast Parallel Algorithms for Short-Range Molecular Dynamics, J. Comput. Phys. **117**, 1 (1995).

[26] A. Strachan, A. C. van Duin, D. Chakraborty, S. Dasgupta, and W. A. Goddard III, Shock waves in high-energy materials: the initial chemical events in nitramine RDX, Phys. Rev. Lett. **91**, 098301 (2003).

[27] L. Liu, Y. Liu, S. V. Zybin, H. Sun, and W. A. Goddard, ReaxFF-lg: Correction of the ReaxFF Reactive Force Field for London Dispersion, with Applications to the Equations of State for Energetic Materials, J. Phys. Chem. A **115**, 11016 (2011).

[28] S. Nosé, A unified formulation of the constant temperature molecular dynamics methods, J. Chem. Phys. **81**, 511 (1984).

[29] W. G. Hoover, Canonical dynamics: Equilibrium phase-space distributions, Phys. Rev. A **31**, 1695 (1985).

[30] P. Giannozzi, S. Baroni, N. Bonini, M. Calandra, R. Car, C. Cavazzoni, D. Ceresoli, G. L. Chiarotti, M. Cococcioni, I. Dabo, and others, QUANTUM ESPRESSO: a modular and open-source software project for quantum simulations of materials, J. Phys. Condens. Matter **21**, 395502 (2009).

[31] D. Vanderbilt, Soft self-consistent pseudopotentials in a generalized eigenvalue formalism, Phys. Rev. B **41**, 7892 (1990).

[32] J. P. Perdew, K. Burke, and M. Ernzerhof, Generalized gradient approximation made simple, Phys. Rev. Lett. **77**, 3865 (1996).

[33] S. Grimme, J. Antony, S. Ehrlich, and H. Krieg, A consistent and accurate ab initio parametrization of density functional dispersion correction (DFT-D) for the 94 elements H-Pu, J. Chem. Phys. **132**, 154104 (2010).

[34] S. Baroni, S. De Gironcoli, A. Dal Corso, and P. Giannozzi, Phonons and related crystal properties from density-functional perturbation theory, Rev. Mod. Phys. **73**, 515 (2001).

[35] Y. Thakur, R. Dong, M. Lin, S. Wu, Z. Cheng, Y. Hou, J. Bernholc, and Q. Zhang, Enhancing the Dielectric Properties of Polymers by Exploring Disordered Structures with Large Free Volumes, (To be published).